DOI https: //doi. org/10.1007/s11595-023-2680-1

Deformation Mechanism of Bimodal Structured 2205 Duplex Stainless Steel in Two Yield Stages

SHENG Jie[1,2,3], DU Mingchen[1], LI Yufeng[2], MA Guocai[1,2], CHEN Weiqian[1,3], ZHENG Yuehong[1], ZHAN Faqi[1], REN Junqiang[1], G I Raab[4], LA Peiqing[1*]

(1. State Key Laboratory of Gansu Advanced Non-Ferrous Metal Materials, Lanzhou University of Technology, Lanzhou 730050, China; 2. Jiuquan Iron and Steel (Group) Co., Ltd., Jiayuguan 735100, China; 3. Key Laboratory of Solar Power System Engineering, Jiuquan Vocational and Technical College, Jiuquan 735000, China; 4. Institute of Physics of Advanced Materials, Ufa State Aviation Technical University, 12 K. Marx Street, Ufa 450008, Russia)

Abstract: A kind of micro/nanostructured 2205 duplex stainless steel (DSS) with uniform distribution of nanocrystals was prepared via aluminothermic reaction method. The analysis of stress-strain curve showed that the fracture strength and elongation of the specimen were 946 MPa and 24.7%, respectively. At present, the research on microstructure of bimodal 2205 DSS at room temperature (RT) mainly depended on scanning electron microscope (SEM) observation after loading experiments. The test result indicates that there are two different yield stages in stress-strain curve of specimen during tensile process. The microstructure of duplex bimodal structured stainless steel consists of two pairs of soft hard regions and phases. By studying deformation mechanism of bimodal structured stainless steel, the interaction between soft phase and hard phase are discussed. The principle of composition design and microstructure control of typical duplex stainless steel is obtained, which provides an important research basis for designing of advanced duplex stainless steel.

Key words: 2205 duplex stainless steel; bimodal structure; *in-situ* tensile test; deformation mechanism; two different yield stages

1 Introduction

Duplex stainless steel (DSS) retained properties of ferrite stainless steel, such as high thermal conductivity, low expansion coefficient and superplasticity[1,2]. By comparing austenitic stainless steel, $\alpha+\gamma$ DSS had higher strength, especially higher yield strength and fatigue strength. 2205 DSS had become the most widely used and the largest amount of DSS so far, which accounted for about 60% of the total use of DSS[3,4]. Generally, 2205 DSS was composed of 22% Cr, 2.5% Mo and 4.5% Ni-N alloy. The solution structure of 2205 DSS normally contained dual phase of ferrite and austenite, and the volume fraction of one phase was not less than 30%. It had high strength, good impact toughness and good overall and local stress corrosion resistance[5,6]. Density of nominal 2205 DSS is 7.8 g/cm^3 and exhibits magnetic. Tensile strength was greater than 750 MPa, while elongation reached 25%, and hardness was 248 HV. The comprehensive mechanical properties of DSS could achieve the best matching when dual phases were half of each other. Therefore, controlling the proportion of dual phase and the stability of microstructure was the key to use of DSS[7,8].

Recent work had demonstrated that duplex phase nanostructure could effectively improve plasticity of nanocrystalline alloys[9-12]. For duplex phase metals with bimodal structure, bonding condition of dual phase interface and microstructure of constituent alloy had an important influence on the overall mechanical properties, deformation behavior and fracture behavior. Macroscopic properties and deformation mechanism were also different from those of single phase alloy[13-15].

2 Experimental

2.1 Materials and electrolyte solution

Alloy used in this study was prepared by alumino-

(Received: May 8, 2022; Accepted: Nov. 27, 2022)

SHENG Jie (盛捷): Assoc. Prof.; Ph D; E-mail: shengj605@163.com

*Corresponding author: LA Peiqing (喇培清): Prof.; Ph D; E-mail: pqla@lut.edu.cn

Funded by the National Natural Science Foundation of China (No.51911530119), the Department of Education of Gansu Province Innovation Fund (No. 2021A-023), and the Open Fund Project of Key Laboratory of Solar Power System Engineering Project (No. 2022SPKL01)

thermic reaction method[16]. The chemical compositions (in wt.%) of the 2205 DSS used in this study were: Cr 7.27, Ni 1.59, Mn 0.40, Al 4.30, Mo 1.50, C 0.001, Si 0.19, N 0.12, and Fe balance. Details of the prepared ingots were given in the previous publication[17-19]. The volume fraction of ferrite area in total area was calculated by Image Pro Plus 6.0 software, which was the volume fraction of ferrite. Ten scanning electron microscopy (SEM) images were selected for statistics under each deformation, and the average value was obtained, which made the results more accurate. The volume fraction of ferrite was 46% and that of austenite was 54%. The volume fraction of austenite and ferrite was 1:1, which achieved the design requirements.

Here, two-step rolling method was used to obtain bimodal structured 2205 DSS. As-cast ingots were treated via hot-rolling operations with 40% thickness reduction at 1 273 K. Multiple passes cold rolling process with 30%, 50%, 70% and 80% thickness reduction at 873 K were performed. According to the previous experiments[20,21], four specimens all had bimodal structure, which could be distinguished by different rolling thickness reduction.

2.2 Tensile tests

Dog-bone shaped tensile specimens were machined by a wire electrical discharge milling, which had a gauge length of 32 mm and 3×1 mm^2. The uniaxial tensile tests were carried out at RT by universal mechanical testing machine (WDW-100D) and the crossing speed was 0.2 mm/min. The tensile direction was parallel to the rolling direction. Each measurement was repeated three times to ensure the reproducibility of results.

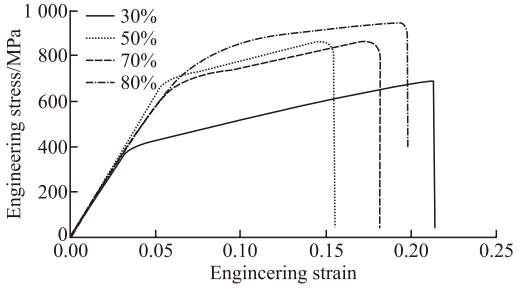

Fig.1 Engineering stress-strain curves for the rolled steel trips with different thickness reduction

The displacement force curves of four kinds of specimens were obtained by uniaxial tensile test, which were converted into corresponding stress-strain curves, as shown in Fig.1. With the rolling thickness reduction increasing from 30%, 50%, 70% to 80%, the tensile strength increased from 691 to 864, 890 and 946 MPa, and the elongation first decreased 28.7% and then increased to 18.9%, 22.6%, 24.7%, respectively. Therefore, the specimen with 80% thickness reduction was selected as test materials, which achieved the best match of strength and plasticity.

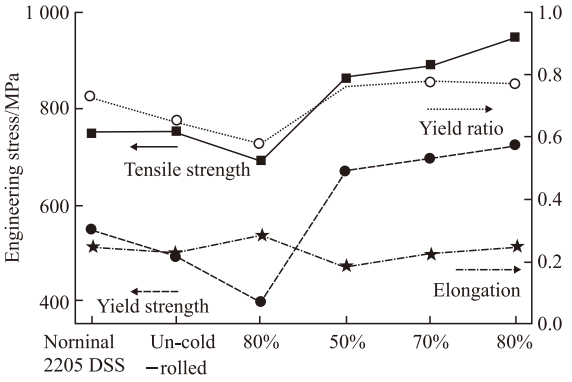

Fig.2 Mechanical properties of 2205 DSS with different bimodal structures at RT

The mechanical properties of 2205 DSS with different thickness reduction at RT was shown in Fig.2. Different rolled steel trips with different thickness reduction corresponded to different microstructure. The red line segment was the tensile strength. It could be seen that the tensile strength of these four different rolling thickness reductions increasing from 30% to 80% showed an upward trend. The tensile strength was as high as 946 MPa. Similarly, yield strength (blue line segment) also showed the same upward trend with change of microstructure. The elongation (green line segment) decreased from 28.7% to 18.9%, and then increased to 24.7%. The result revealed that strength and plasticity of bimodal structured specimen with rolling thickness reduction 80% reached best matched and the yield ratio (black line segment) was 0.77.

2.3 *In-situ* SEM tension experiments

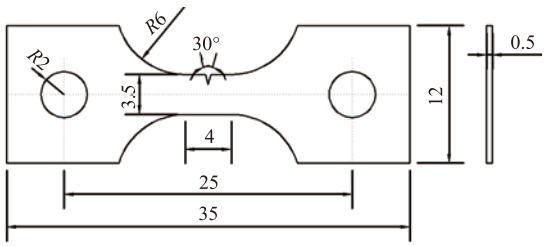

Fig.3 The dimension of *in-situ* tensile specimens (unit: mm)

The specimen was cut from the plate of the rolled bimodal structured 2205 DSS with 80% thickness reduction along the rolling direction. The size of specimens was shown in Fig.3[9]. Specimens for optical microscopy (OM, Mef3) and SEM (FEI Quanta 450) were etched with 4 g $CuSO_4$ + 20 mL HCl + 20 mL H_2O for

5 s. The microscopic deformation and fracture behavior was observed using a dynamic tensile device (MTEST 2000) in SEM at a constant crossing speed of 0.2 mm/min at RT[22]. In the process of *in-situ* tensile test, SEM was used to observe the loads and crack propagation.

3 Results

3.1 Microstructure

Typical microstructures of bimodal structured 2205 DSS specimen with 80% thickness reduction are shown in Fig.4. The most of gray white dendritic areas are ferrite and others are dark austenite. As observed in Fig.4, the thickness distribution of ferrite are more uniform under the effect of rolling force, and the austenite phase and ferrite phase are arranged alternately. This is a typical heterogeneous layered dual phase microstructure.

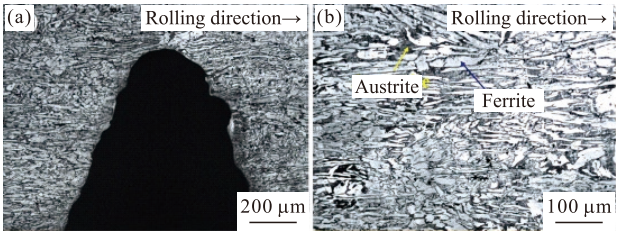

Fig.4 Typical OM images of specimen

3.2 Observation of deformation behavior during *in-situ* tensile test

The whole process of deformation of the specimen surface during *in-situ* tensile test is presented in Fig.6. The surface of the specimen is smooth before the tensile loading is applied in Fig.6(a). In Fig.6(b), when the tensile stress reaches 822 MPa, the main crack is very bent, and intensive slip lines can be observed when the main crack is magnified to 1 000 times near the crack location. At this time, the tensile stress is 868 MPa, as shown in Fig.6(c), and a small crack appears at the top right of the main crack, and its propagation direction is the same as that of the main crack. When the crack tip is magnified 2 000 times, obvious slip bands can be observed, and the slip band direction is almost at an angle of 45º to the crack direction. The main crack changes its propagation direction at the slip band at the lower end of the crack, bends and connects with the crack. The tensile stress reaches 830 MPa in Fig.6(d). It can be observed that another crack above the main crack is developing at the same time. Along the intensive slip line, these two cracks are connected, and surface near the crack has presented uneven orange peel fold. In Fig.6(e), when the tensile stress reaches 892 MPa, slip lines near main crack are still intensive and short, and slip lines at the front of main crack are obvi-

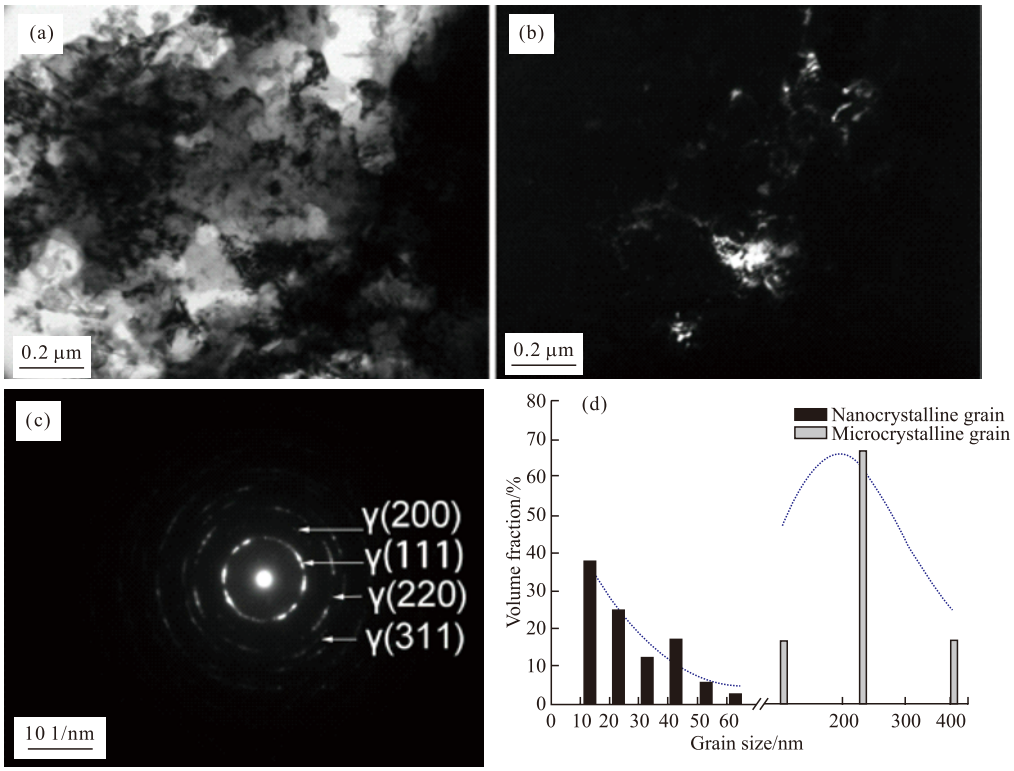

Fig.5 Typical TEM images and grain size distribution: (a) bright-field TEM image; (b) dark-field TEM image; (c) selected area electron diffraction image and (d) statistical figure of grain size distribution

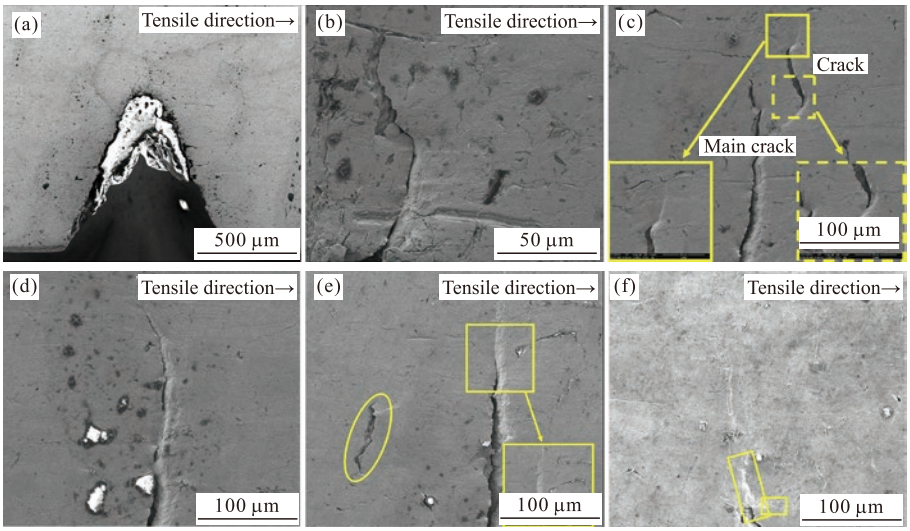

Fig.6 Deformation behavior of specimen surface

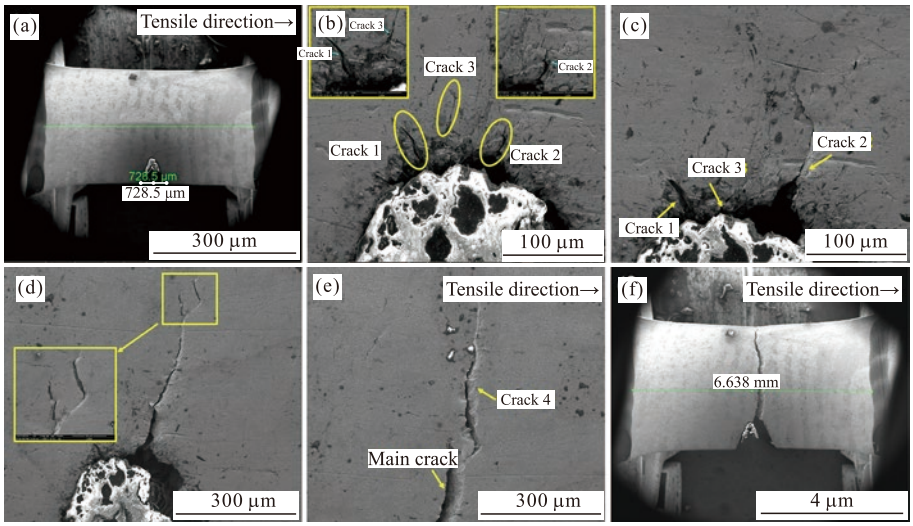

Fig.7 Crack propagation in specimens

ous. The internal deformation is severe, which makes the surface at the tip of the main crack uneven. At the same time, there is a small crack on the side of main crack and propagates in the same direction. The specimen is on the verge of fracture in Fig.6(f). The deformation at the tip of main crack is obvious, the slip band is intensive, and the main crack extends along the direction of intensive slip lines and passes through an inclusion.

3.3 The feature of fatigue crack propagation during *in-situ* tensile test

Crack initiation and propagation process of bimodal structured 2205 DSS specimen with 80% thickness reduction during *in-situ* tensile test is represented in Fig.7. It shows the whole process of crack initiation, propagation, instability and fracture. There are two possible propagation paths at the tip of microcrack. The first is that the microcracks are passivated, sharpened and propagated along slip lines. The second is that microcrack will propagate along phase boundary in the form of interface separation.

Fig.7(a) illustrates that the flatness near the prefabricated U-type notch can be observed before loading. When the tensile stress reaches 685 MPa, three microcracks appears at the root of the notch, among which Crack 1 and Crack 2 are more obvious, and they starts to crack from the root of the U-type notch, as shown in Fig.7(b). Crack 3 is a newly developed crack, which is smaller than the other two crack initiation microcracks, and starts from the middle of the specimen. The white block in the notch is a small amount of copper replaced by the corrosion solution, which is suspended and attached to the notch, where the copper and the sample can be peeled off. In Fig.7(c), the above three microcracks develop at the same time with the continuous application of tensile loading. When the tensile stress is 795 MPa, Crack 2 propagation speed

is obviously accelerated, and the propagation path is also very bent. When tensile stress is 888 MPa, Crack 2 has fully developed into main crack, and the main crack propagation path is approximately arc-shaped in Fig.7(d). A new microcrack of Crack 4 appears in the upper right corner of the main crack tip. When loading reaches 875 MPa, main crack and Crack 4 still expand separately and are not connected. The propagation speed of Crack 4 is faster than that of the main crack, and there are three inclusions above Crack 4, as shown in Fig.7(e). Crack 4 continues to expand through the nearest inclusion. The specimen is completely fractured after instability in Fig.7(f).

4 Analysis and discussion

4.1 Influence of bimodal structure on deformation behavior for 2205 DSS

The two different yield stages is observed in engineering stress-strain curve of bimodal structured 2205 DSS specimen with 80% thickness reduction in Fig.8. Obviously, there are two kinds of slope line segments on the curve. As tensile stress within 0-582 MPa, tensile curve is basically a straight line (red), and a small bend occurs at 582 MPa. When tensile stress exceeds 582 MPa, another straight line (green) develops with a new slope in the range of 582-724 MPa. The first slope straight line represents that yield has occurred once, and the strain hardening occurred in microcrystalline region. When tensile stress reaches 582 MPa, NGs begin to get involved yield. Then deformation occurs severely, in both microcrystalline region and nanocrystalline region. When tensile stress exceeds 582 MPa, it leads to deformation failure of microcrystalline grains. At this time, boundary sliding of NGs becomes the main deformation mode, which results in secondary yield. When tensile stress exceeds 946 MPa, it has reached the tensile strength of NGs and microcrystalline grains, and specimen begins to bend and fracture.

According to Taylor's strength theory, the strain hardening is mainly due to dislocation slip in coarse grains and NGs. Comparing with NGs, dislocations are easier to slip in microcrystalline grains, so microcrystalline grains can provide more toughness. Nanocrystalline matrix has greater loading in the load bearing aspect. Only a small part of loading is transferred to microcrystalline grains. Therefore, the volume fraction of microcrystalline grains increases but strength decreases little. In addition, stress concentration in nanocrystalline matrix can be released by microcrystalline grains. It can be seen from *in-situ* tensile test curve that hardening ability increases with increase of the volume fraction for microcrystalline grains. The main reason is that the hardening of nanocrystalline materials is mainly caused by dislocations accumulation of at grain boundaries. The number of dislocations decreases in the specimen because of grain size of NG is very small. The difference in mechanical properties of bimodal structure is generally considers to be the main reason for multi-stage work hardening behavior in bimodal structured DSS[24,25]. In process of tensile deformation, the softer austenite phase (soft phase) first yield and plastic deformation occurs, while the harder ferrite phase (hard phase) is still in the stage of elastic deformation. With continuing tension and increasing deformation, the austenite phase becomes work hardening, which results in the ferrite phase plastic deformation, and dual phase ultimately enters the stage of co-ordinated deformation. Compared with the difference in hardness between microcrystalline grains and NGs, the hardness difference between austenite phase and ferrite phase is small. Therefore, deformation at the early stage (the corresponding strains were not more than 1%, pink line in Fig.8), dual phase coordinated deformation is completed. In addition, the bimodal structure of DSS also results in the inhomogeneity of mechanical properties. Couples with the variety of deformation mechanism for each phase have a fundamental influence on the work hardening ability for specimen.

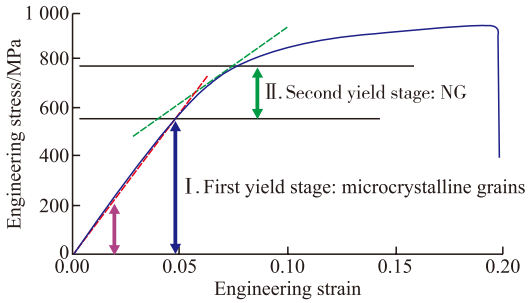

Fig.8 Two different yield stages in engineering stress-strain curve

When tensile stress is in the range of 0-126 MPa, deformation behavior is mainly the coordinated deformation of austenite and ferrite. The austenite phase first yields and causes plastic deformation. With increasing of deformation, austenite phase is continuously work hardening, which leads to ferrite phase plastic deformation. When tensile stress is in the range of 126-582 MPa, the soft microcrystalline phase yields and produces plastic deformation, while the hard nanocrystalline regions are still in the elastic deformation stage. With the further increasing of deformation, work hardening

occurs in microcrystalline regions. And ultimately, this leads to the plastic deformation of grain boundary sliding in nanocrystalline regions. At this time, microcrystalline regions and nanocrystalline regions enter the stage of co-ordinated deformation. It is known that the multi-stage hardening is macroscopic consequence of coordination and competition among various deformation mechanisms[26]. However, it is generally believed that the main reason for the multi-stage hardening behavior is the difference in microscopic mechanical properties of component with dual phase structure.

4.2 The interaction between duplex bimodal structure and mechanical behavior

Generally, austenite phase is soft phase and ferrite phase is hard phase in DSS at RT. However, the austenite phase is hard and the ferrite phase is soft at high temperature[23]. The different deformation mechanisms of the duplex phases cause to the uneven distribution of strain and stress, and eventually lead to different fracture mechanisms[27].

4.2.1 Deformation mechanisms for duplex bimodal structured metals

The microstructure of duplex bimodal structured metals includes the soft region composed of microcrystalline phase, the hard region composes of nanocrystalline phase and the austenite phase (soft phase) and ferrite phase (hard phase) in their respective structures. It consists of two pairs of soft hard regions and phases, which together constitutes the microstructure of dual phase and bimodal structure.

After large deformation rolling with 80% deformation, nanocrystalline austenite grains and nanocrystalline ferrite grains are uniformly dispersed in microcrystalline structure. Austenite microcrystalline grains and ferrite microcrystalline grains of soft phase have obvious plastic deformation during rolling, which is beneficial to fill the gap between NGs. Microcrystalline grains have good plasticity, while NG provides poor plasticity and crack propagation resistance in duplex bimodal structured metals.

2205 DSS is located in dual phase region. Due to the different stacking fault energies of FCC austenite and BCC ferrite, its deformation behavior is very complex[28]. Stacking fault energy of bcc ferrite is high, and the deformation mechanism is mainly dislocation slip. According to different stacking fault energy, the deformation mechanism is different. With decreases of stacking fault energy, the deformation mechanisms are dislocation slip, twinning and strain-induced martensitic transformation. Therefore, it can be inferred that deformation of DSS is mainly controlled by austenite phase, and multi-stage hardening characteristics are mainly related to multi mechanism plastic deformation of austenite phase. The hardening rate of DSS is higher than ASS because plastic deformation of various phases in DSS is not uniform. The different deformation mechanism of dual phases results in uneven distribution of strain and stress in each phase. Especially for dual phase metals with different properties, anisotropy in grains increases obviously with decrease of grain size.

In the of early stage of deformation for DSS, the soft γ austenite phase is strain control phase, in which plastic deformation occurred firstly, while α ferrite phase is still in elastic deformation stage, as shown in Fig.9(a). As Fig.9(b) indicated, dislocations generated in austenite phase are difficult to cross phase boundary and accumulates near phase boundary because of being constrained by hard phase of α ferrite around, which results in back stress at junction of dual phase. The back stress makes it more difficult for dislocations to move from soft γ austenite phase to hard α ferrite phase. Austenite phase is hardened continuously with the increase of deformation, which results in plastic deformation of α ferrite phase in Fig.9(c). Finally, dual phase deforms at the same strain rate. The hardness difference between austenite phase and ferrite phase is small, so strains corresponding to turning point of deformation of both phases are less than 1%. But for DSS, both austenite and ferrite are deformable plastic phases, and difference of mechanical properties between them is relative-

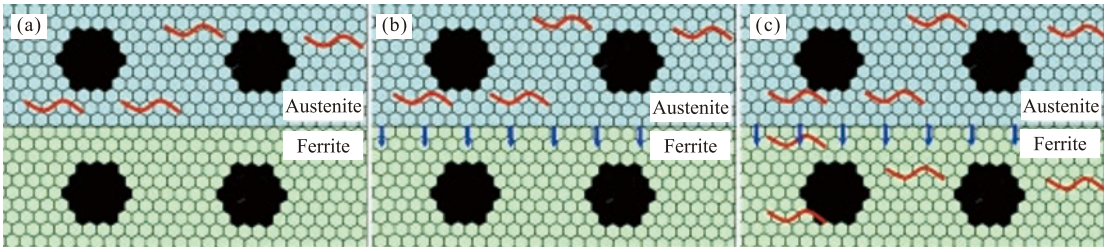

Fig.9 Diagram of deformation coordination process of dual phase steel during stretching

ly small. No matter which phase had priority of plastic deformation, once hardness of the first deforms phase exceeded the other phase by work hardening, the latter will also have plastic deformation. And so on, hardness of dual phase increases with increasing of strain.

As the deformation continues, the work hardening ability of austenite phase and ferrite phase is different. This difference makes work hardening behavior changed again. Therefore, in homogeneity of micromechanical properties of DSS, diversification of deformation mechanism for each phase, has a fundamental impact on overall work hardening behavior. When grain size of dual phase decreases to submicron or even nanoscale, hardness difference between austenite phase and ferrite phase also increases. At this time, it can not provide effective work hardening ability because of small grain size. Meanwhile, local stress concentration caused by hardness difference between dual phases in deformation process, can not be effectively relaxed, which further weakens the overall plasticity of material. This further weakens the overall plasticity of material. Therefore, dual phase material lacks sufficient strain coordination on nanoscale, and shows a single work hardening characteristic with a high work hardening index. Dislocation density is very low and mainly distributes near grain boundaries in nanocrystalline phase. The austenite phases at boundary have relatively high initial hardness, so the dislocations mainly accumulate on the side near ferrite phase. Duplex bimodal structure has a variety of micro plasticity response. The difference of microstructure mechanical behavior of different structural components effectively promotes the generation of local strain gradient, which provides favorable conditions for the generation of back stress. The internal stress produced by the interaction between phase boundary and dislocation in turn strengthens hindering effect of phase boundary on dislocation. The results reveal that back stress produced during deformation of dual phase structure metal have a significant contribution to the overall strength and work hardening for specimen.

4.2.2 Fracture mechanism for duplex bimodal structured metals

The crack first nucleates on phase boundary and propagates along it. There is no obvious crack in austenite phase. Cracks cross through austenite grains and then propagates into ferrite grains. Austenite grains have a certain inhibitory effect on crack propagation. This is because FCC austenite phase are soft and easy to deform at RT, while BCC ferrite phase are hard and difficult to deform. This results in uneven distribution of strain and deformation difference at phase boundary. When the deformation difference is large enough, dual phase slid at phase boundary, and then cracks diffuse along it.

Propagation direction of microcrack tip is mainly controlled by both slip bands induced by bimodal structure and crack along dual phase interface in bimodal structured DSS. In the early stage of *in-situ* tensile test, microcracks form in nanocrystalline matrix. With tensile load increasing, it is easy to produce dislocation accumulation deformation and slip deformation into slip band in microcrystalline region. Tip of microcrack will slip in microcrystalline region, passivate, sharpen and continue to expand to nanocrystalline region. Along with the increase of voids on the interface, strength of the interface weakens, and crack is easier to propagate along interface, which leads to ultimate fracture for the specimen. After grain refinement, grain boundary density and phase boundary density of bimodal structured specimen with rolling thickness is reduced by 80%, which further enhances hindering effect of phase boundary on dislocation and increases strength.

During deformation of DSS, strength of austenite grains is lower and softening ability is stronger. The total strain of austenite grains is much larger than ferrite grains at the initial stage of deformation. Therefore, plastic deformation behavior of DSS at the initial stage of deformation is dominated by austenite grains. At the initial stage of deformation, high stacking faults of ferrite grains can promote cross slip of deformed dislocations, which is called dynamic recovery effect. For austenite grains, the stacking fault energy is low, width of spreading dislocation is wide, and it is difficult to cluster. The deformation sequence and deformation amount of dual phase are different in DSS, which leads to different dislocation density on both sides of grain boundary.

5 Conclusions

a) The bimodal structured 2205 DSS specimen with 80% thickness reduction obtained high strength of 946 MPa and good plasticity of 24.7%. There were two different yield stages in engineering stress-strain curve. As tensile stress within 0-582 MPa, strain hardening occurred in microcrystalline region. When tensile stress reached in range of 586-724 MPa, NGs get involved yield. With the increase of tensile stress 582 MPa, microcrystalline grains would deform and fail. The main

deformation mode was grain boundary sliding of NGs, which resulted in secondary yield. When tensile stress exceeded the tensile strength 946 MPa, the specimen began to bend and fracture.

b) Bimodal structured 2205 DSS had good plasticity, and the surface presented orange fold after fracture. The fracture mode was composed of tearing fracture, opening fracture and sliding fracture. The mismatching of microstructure and properties on both sides of phase boundary would inevitably lead to uncoordinated deformation and stress concentration.

c) The microstructure of duplex bimodal structured metals included the soft region composed of microcrystalline phase and the hard region composed of nanocrystalline phase. The austenite phase (soft phase) and ferrite phase (hard phase) contained in their respective structures. It consisted of two pairs of soft hard regions and phases. Owing to mechanical property differences between austenite and ferrite, DSS exhibited multiple microscopic plastic responses during tensile deformation. Propagation direction of microcrack tip was affected by both slip bands induced by bimodal structure and cracked along dual phase interface.

References

[1] Gunn RN. *Duplex Stainless Steels: Microstructure, Properties and Applications*[M]. Cambridge: Abington Publishing, 1997

[2] Lei Y, Huang SY, Meng ZH, *et al*. Effects of Biaxial Tensile on the Deformation Behavior of DP590 High-strength Steel Sheet under High Strain Rate[J]. *J. Wuhan Univ. Technol.-Mater. Sci. Ed.*, 2017, 32(6): 1 441-1 445

[3] Zhao Y. *Evolutions of As Cast Structures and Mechanisms of High Temperature Phase Transformation in Nirtogen Bearing Duplex Stainless Steel*[D]. Beijing: University of Science and Technology Beijing, 2017

[4] Yang XJ, Ling X, Wang DX, *et al*. Deformation Behavior and Formability of Gradient Nano-grained AISI 304 Stainless Steel Processed by Ultrasonic Impact Treatment[J]. *J. Wuhan Univ. Technol.-Mater. Sci. Ed.*, 2017, 32(5): 1 147-1 155

[5] Wu J. *Duplex Stainless Steel*[M]. Beijing: Metallurgical Industry Press, 1999

[6] Koga N, Nameki T, Umezawa O, *et al*. Tensile Properties and Deformation Behavior of Ferrite and Austenite Duplex Stainless Steel at Cryogenic Temperatures[J]. *Mat. Sci. Eng. A-Struct.,* 2021, 801: 140 442

[7] Chao DY, Xu RG, Sun YZ, *et al*. Effect of Aging Treatment at 850 ℃ on Microstructures and Mechanical Properties in Duplex Stainless[J]. *Mater. Rep.,* 2019, 33: 369-372

[8] Pang QH, Zhao ZD, Xu M, *et al*. Plastic Deformation Mechanism of Dual-phase Steel at Different Strain Rates[J]. *J. Wuhan Univ. Technol.-Mater. Sci. Ed.*, 2020, 35(6): 1 142-1 148

[9] Sheng J, Jin J, Shi Y, *et al*. Superior Strength and Ultrahigh Ductility in Hierarchical Structured 2205 Duplex Stainless Steel from Nanoscale to Microscale[J]. *Mater. Trans.*, 2021, 62(11): 1 604-1 608

[10] Sheng J, Su JQ, La PQ, *et al*. Process of *In-situ* Study on Mechanical Properties for Micro/nano-structured Alloy[J]. *J. Nanoelectron. Optoe.,* 2018, 13(5): 637-645

[11] YANG T, ZHAO YL, LI WP, *et al*. Ultrahigh-strength and Ductile Superlattice Alloys with Nanoscale Disordered Interfaces[J]. *Science*, 2020, 369(6502): 427-432

[12] KOU H, LU J, LI Y. High High-strength and High-ductility Nanostructured and Amorphous Metallic Materials[J]. *Adv. Mater.,* 2014, 26(31): 5 518-5 524

[13] Naser H, Deschamps A, Mantel M, *et al*. Architectured Duplex Stainless Steel Micro-composite: Elaboration and Microstructure Characterization[J]. *Mater. Design*, 2018, 145: 156-167

[14] Haghdadi N, Cizek P, Hodgson PD, *et al*. Microstructure Dependence of Impact Toughness in Duplex Stainless Steels[J]. *Mat. Sci. Eng. A-Struct.,* 2019, 745: 369-378

[15] Shi YR, Yuan GJ, Guo SJ. Micromechanics Finite Element Analysis of Local Micro-deformation Behaviour of Duplex Stainless Steel under Uniaxial Tension[J]. *Chin. Q. Mech.,* 2020, 41: 29-38

[16] Shi Y, Song Y, La PQ, *et al*. Lamella Multiple Grained Structure Making 2205 Duplex Stainless Steel with Superior Strength and Ductility[J]. *J. Wuhan Univ. Technol.-Mater. Sci. Ed.*, 2021, 36(5): 754-760

[17] Sheng J, La PQ, Su JQ, *et al*. *In Situ* SEM Analysis for Deformation Mechanism of Micro/nanostructured 304 Stainless Steel with High Strength and Good Plasticity[J]. *Mod. Phys. Lett. B,* 2018, 32(17): 1 850 182

[18] Sheng J, Wei JF, Li ZN, *et al*. Micro/nano-structure Leads to Super Strength and Excellent Plasticity in Nanostructured 304 Stainless Steel[J]. *J. Mater. Res. Technol.,* 2022, 17: 404-411

[19] Shi Y, Yuan MW, Li ZN, *et al*. Two-step Rolling and Annealing Makes Nanoscale 316L Austenite Stainless Steel with High Ductility[J]. *Mat. Sci. Eng. A-Struct.,* 2019, 759: 391-395

[20] Zheng YH, Zhao H, Zhang N, *et al*. Effect of Excessive Fe_2O_3 on Microstructural Evolution of Micro/nanocrystalline 2205 Duplex Stainless Steel Prepared by Aluminothermic Reaction[J]. *Front. Mater.,* 2020, 7: 1-12

[21] Fu J, Tang MK, Zhang QX. Simple Fabrication of Hierarchical Micro/Nanostructure Superhydrophobic Surface with Stable and Superior Anticorrosion Silicon Steel via Laser Marking Treatment[J]. *J. Wuhan Univ. Technol.-Mater. Sci. Ed.*, 2020, 35(2): 411-417

[22] Chen AY, Ruan HH, Wang J, *et al*. The Influence of Strain Rate on the Microstructure Transition of 304 Stainless Steel[J]. *Acta Mater.,* 2011, 59(9): 3 697

[23] Liu YY. *Study on Microstructure and Property Evolution of LDX 2101 during Thermal Deformation*[D]. Hangzhou: Zhejiang University, 2013

[24] WU XL, JIANG P, CHEN L, *et al.* Extraordinary Strain Hardening by Gradient Structured[J]. *Proc. Natl. Acal. Sci. USA*, 2014, 111(20): 7 197-7 201

[25] ZHAO J, KAN Q, ZHOU L, *et al.* Deformation Mechanisms Based Constitutive Modeling and Strength-ductility Mapping of Gradient Nano-grained Materials[J]. *Mat. Sci. Eng. A-Struct.,*2019, 742: 400-408

[26] WU G, CHAN KC, ZHU LL, *et al*. Dual-phase Nanostructuring as a Route to High-strength Magnesium Alloys[J]. *Nature,* 2017, 545(7 652): 80-83

[27] CHEN XD, HOU XH, BAI PC, *et al. In Situ* Electron Microscopic Observation of Crack Propagation in Two-Stage Aging Sample of Spray-Deposited Al-Zn-Mg-Cu Alloy[J]. *Chinese J. Rare Metals,* 2021, 45(11): 1 403-1 408

[28] SHENG J, LI JC. Laguerre Simulation and Visualization for Microstructure of Metal Materials[J]. *J. Wuhan Univ. Technol.-Mater. Sci. Ed.*, 2014, 29(1): 164-167